Internal Electron Transfer and Structural Dynamics of cd_1 Nitrite Reductase Revealed by Laser CO Photodissociation†

Emma K. Wilson,‡ Andrea Bellelli,‡ Susanna Liberti,‡ Marzia Arese,‡ Sabrina Grasso,‡ Francesca Cutruzzolà,‡ Maurizio Brunori,*,‡ and Peter Brzezinski§

Dipartimento di Scienze Biochimiche and Centro di Biologia Moleculare del CNR, Università di Roma "La Sapienza", 00185 Roma, Italy, and Department of Biochemistry, The Arrhenius Laboratories for Natural Sciences, Stockholm University, SE-10691, Stockholm, Sweden

Received January 25, 1999; Revised Manuscript Received March 30, 1999

ABSTRACT: Laser photolysis techniques have been employed to investigate the internal electron transfer (eT) reaction within *Pseudomonas aeruginosa* nitrite reductase (*Pa*-NiR). We have measured the ($d_1 \rightarrow c$) internal eT rate for the wild-type protein and a site-directed mutant (*Pa*-NiR H327A) which has a substitution in the d_1-heme binding pocket; we found the rate of eT to be fast, $k_{eT} = 2.5 \times 10^4$ and 3.5×10^4 s^{-1} for the wild-type and mutant *Pa*-NiR, respectively. We also investigated the photodissociation of CO from the fully reduced proteins and observed microsecond first-order relaxations; these imply that upon breakage of the $Fe^{2+}-CO$ bond, both *Pa*-NiR and *Pa*-NiR H327A populate a nonequilibrium state which decays to the ground state with a complex time course that may be described by two exponential processes ($k_1 = 3 \times 10^4$ s^{-1} and $k_2 = 0.25 \times 10^4$ s^{-1}). These relaxations do not have a kinetic difference spectrum characteristic of CO recombination, and therefore we conclude that *Pa*-NiR undergoes structural rearrangements upon dissociation of CO. The bimolecular rate of CO rebinding is 5 times faster in *Pa*-NiR H327A than in the wild-type enzyme (1.1×10^5 M^{-1} s^{-1} compared to 2×10^4 M^{-1} s^{-1}), indicating that this mutation in the active site alters the CO diffusion properties of the protein, probably reducing steric hindrance. CO rebinding to the wild-type mixed valence enzyme ($c^{3+}d_1{}^{2+}$) which is very slow ($k = 0.25$ s^{-1}) is proposed to be rate-limited by the $c \rightarrow d_1$ internal eT event, involving the oxidized d_1-heme which has a structure characteristic of the fully oxidized and partially oxidized *Pa*-NiR.

Nitrite reductases (NiRs)[1] play an important role in the dissimilative denitrification chain of facultative anaerobic bacteria where they catalyze the reduction of nitrite to NO ($NO_2^- + 2H^+ + e^- \rightarrow NO + H_2O$). These enzymes fall into two distinct classes depending on the cofactor employed: one class containing copper (Cu-NiRs) and the other containing two heme centers (cd_1-NiRs). Enzymes of the latter class are homodimers (subunit molecular mass 60 kDa), each subunit containing one *c*-type heme and one unique d_1-heme; the *c*-heme accepts electrons from external donors (such as cytochrome *c*551 and azurin) whereas the d_1-heme is the site of nitrite binding and catalysis (see refs *1*−*4* for reviews). After *c*-heme reduction, one electron is transferred in a slow intramolecular electron transfer (eT) process (0.25 s^{-1}) to the d_1-heme (*5*). Following NO_2^- binding, the d_1-heme donates an electron to the substrate, and it is postulated that two histidine residues (His327 and His369 in *Pa*-NiR; see Figure 1) are involved in a protonation reaction coupled to the removal (as water) of one oxygen atom from nitrite (*6*, *7*). At this stage of the reaction, NO is bound to the oxidized d_1-heme, and its dissociation before the rereduction of the d_1-heme (by the *c*-heme) is a critical step in the catalytic cycle, which if not completed results in a "dead-end" $Fe^{2+}-NO$ complex as NO is able to bind ferrous d_1-heme with an extremely high affinity (*3*, *8*, *9*). Another interesting property of cd_1-NiRs is that they are also able to catalyze the four-electron reduction of O_2 to water, albeit with a lower efficiency (*10*, *11*).

The three-dimensional structures of *P. aeruginosa* NiR (*Pa*-NiR) (*6*, *12*) and *P. denitrificans* GB17 (formerly known as *T. pantotropha*) NiR (*Pd*-NiR) (*7*, *13*) have provided fundamental information about the amino acid residues involved in catalysis and the protein environment of both heme groups. Each monomer consists of a flexible N-terminal arm and two domains: a cytochrome *c* like domain that contains the *c*-heme, and a β-propeller domain that houses the d_1-heme. Striking features are that in the oxidized form the two enzymes employ different ligands for both redox centers and that upon reduction structural reorganizations are observed, an unusual property for redox proteins (see Figure 1). In oxidized *Pd*-NiR, the *c*-heme ligands are His17 and His69, but upon reduction His17 is replaced by Met106; in contrast, the *c*-heme in *Pa*-NiR is His51 and

† This work was funded by grants from the European Union (Contract BIO4-CT96-0281), the MURST of Italy (P. N. Biologia Strutturale 1998), and CNR PF Biotecnologie (Contract CT97.01084.49). E.K.W. is the recipient of a Human Frontier Science Program Organization long-term research fellowship.

* To whom correspondence should be addressed at the Dipartimento di Scienze Biochimiche, Università di Roma "La Sapienza", P. le A. Moro 5, 00185 Roma, Italy. Fax: 39-06-4440062. Telephone: 39-06-4450291. Email: brunori@axrma.uniroma1.it.

‡ Università di Roma "La Sapienza".

§ Stockholm University.

[1] Abbreviations: NiR, nitrite reductase; *Pa*-NiR, *Pseudomonas aeruginosa* NiR; *Ps*-NiR, *Pseudomonas stutzeri* NiR; *Pd*-NiR, *Paracoccus denitrificans* GB17 NiR; eT, electron transfer; Mb, myoglobin; Hb, hemoglobin; PCR, polymerase chain reaction.

10.1021/bi990179u CCC: $18.00
Published on Web 05/20/1999

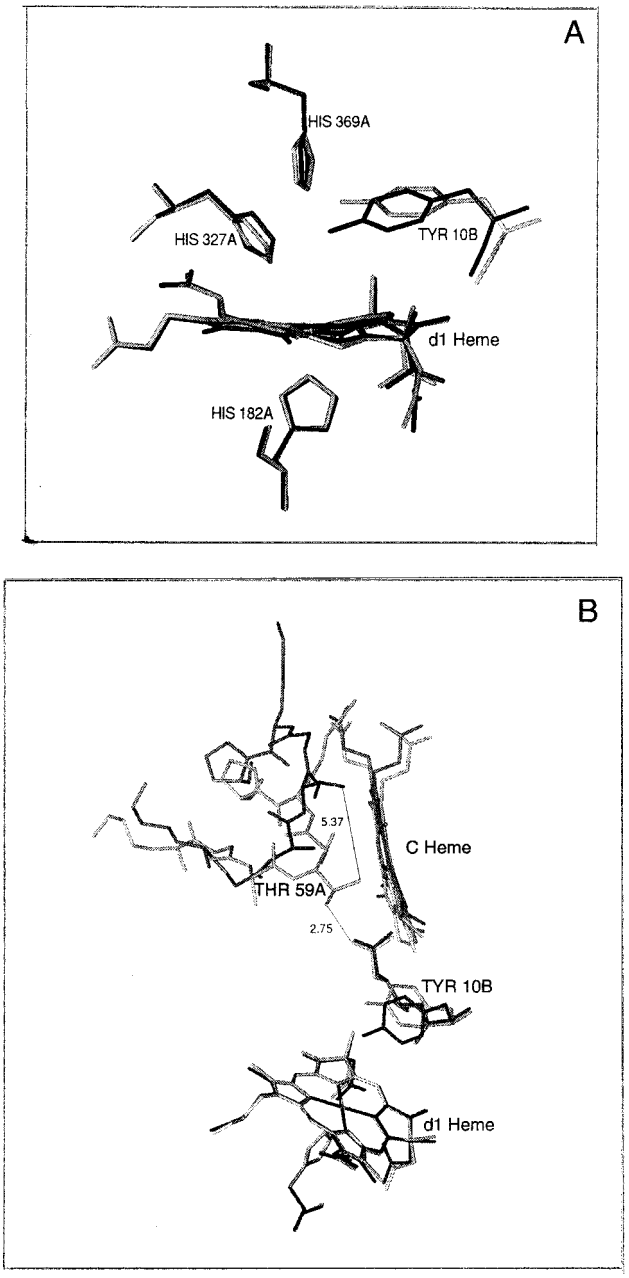

FIGURE 1: Molecular graphics representation of oxidized *Pa*-NiR (depicted in black) superimposed on the structure of reduced unliganded *Pa*-NiR (depicted in gray). The lettering A and B refers to monomer A and monomer B of *Pa*-NiR. Panel A: The d_1-heme active site; the side chains His327, His369, and Tyr10 are shown, and the movement of Tyr10 upon d_1-heme reduction can be seen. Panel B: The conformational change in the *c*-domain 56A−62A loop and the movement of Tyr10 upon reduction of the d_1-heme.

Met88 coordinated in both redox states. The ferric d_1-heme of *Pd*-NiR is liganded by two protein residues, namely, His200 and Tyr25, the latter being part of the N-terminal arm of the same monomer. However, in *Pa*-NiR, the ligands are His182 and a hydroxide ion; the Tyr residue (Tyr10) in the active site of the oxidized enzyme belongs to the N-terminal arm of the other monomer due to "domain swapping" (*6*). Reduction of *Pd*-NiR is accompanied by very large structural rearrangements (*13*); for *Pa*-NiR, the structural alterations are not so extreme, but (as illustrated in Figure 1) there is a concerted movement in which a *c*-domain loop moves 6 Å, Tyr10 rotates (4.2 Å) away from the d_1-heme, and the sixth d_1-heme ligand, a hydroxide ion, leaves the active site, thereby "opening" the distal pocket of the d_1-heme (*12*). Recent crystallographic work on a redox intermediate of *Pa*-NiR has shown that the reduction of the *c*-heme is not associated with these structural changes (*14*).

Our aims have been to investigate the internal electron transfer reaction in cd_1-NiRs using laser photodissociation of the CO complex (*15*), a far reaching approach which can be extended to initiate eT reactions within enzymes in the crystalline state. cd_1-NiRs represent ideal candidates for intramolecular eT studies, as they are well characterized from a structural and functional viewpoint. However, the internal eT event in *Pa*-NiR is known to be complex. Under many experimental conditions, the intramolecular electron transfer is slow (*5*, *9*); but it is variable, and, for example, when O_2 is the final electron acceptor, intramolecular eT rates in excess of 100 s^{-1} have been reported (*16*). Indeed, the structures of *Pa*-NiR and *Pd*-NiR demonstrate that the two hemes are relatively close to one another (edge-to-edge distance is 11.4 Å in *Pa*-NiR) and therefore distance alone does not account for the low rate constant assigned to the intramolecular eT. Moreover, it has been demonstrated that intramolecular eT can be very fast when induced under nonphysiological conditions, for example, by photoexcitation of an enzyme derivative containing a Zn-protoporphyrin IX in the place of the d_1-heme (*17*), or by pulse radiolysis (*18*).

To probe the $d_1 \rightarrow c$ eT event in *Pa*-NiR, we have investigated the valence hybrid derivative $c^{3+}d_1^{2+}$−CO, which upon photolytic breakdown of the Fe−CO bond yields the species $c^{3+}d_1^{2+}$. This is able to transfer an electron to the oxidized *c*-heme, but as the *c*- and d_1-hemes, in the absence of external ligands, share similar redox potentials (approximately +280 mV) (*19*, *20*), the eT reaction produces a mixture of the valence hybrids $c^{3+}d_1^{2+}$ and $c^{2+}d_1^{3+}$. Using this approach, we have measured for the photolytic intermediate a fast internal eT at 2.5×10^4 s^{-1}, and discuss this result with reference to the various redox states of *Pa*-NiR (*6*, *12*, *14*). Preliminary to this approach, we investigated the relaxations, which follow photodissociation of CO bound to fully reduced *Pa*-NiR. The time evolution of the photoproduct proved to be complex, due to microsecond relaxations which, on the basis of spectral analysis, are not geminate rebinding but assigned to structural changes of the reduced d_1-heme active site. We extended our investigations to a site-directed mutant of *Pa*-NiR (H327A), in which one of the two histidine residues in the d_1-heme pocket possibly involved in the protonation and dehydration of bound nitrite (Figure 1) has been mutated to Ala. As demonstrated below, *Pa*-NiR H327A displays a different kinetic behavior from wild-type *Pa*-NiR, which makes it more suitable to the study of photoinduced intramolecular eT and allows us to postulate a role for H327.

EXPERIMENTAL PROCEDURES

Mutagenesis. Mutagenesis of His327 was performed on the *nirS* gene which has been cloned into the vector pUC 19 (pUC-NR). The introduction of the mutation was achieved by PCR methods; three oligonucleotides were synthesized: [I], 5′- GCGGCGCCGTTCCTCGCCGACGGCGGCTGGG-3′; [II], 5′- GCCACGCCCCGGGGCCGGGGTCTTGC-CCACGTCG-3′; and [III], 5′- CCCCGAGTTCATCGT-CAACGTGAAGAAGACCGG-3′. Oligonucleotide [I] is the

mutagenic oligonucleotide. A 160 bp fragment was synthesized by PCR using oligonucleotides [I] and [II] as primers and *pfu* polymerase (Stratagene) (annealing temperature 65 °C); then this fragment was used as a primer in a second PCR step along with oligonucleotide [III]. The second PCR step synthesized a 250 bp fragment using Zyme polymerase (Finn Zyme) (annealing temperature 55 °C). The 250 bp fragment was digested with *Eco*RV and *Bsm*FI and following purification was subcloned into pUC-NR in place of the corresponding wild-type region. The putative mutants were screened by dideoxy DNA sequencing using Sequenase 2.0 reagents (US Biochemicals), and after positive identification, the region between the restriction sites *Eco*RV and *Bsm*FI was completely sequenced to ensure that no PCR errors were present. The entire mutant gene was then subcloned into the expression vector pNM-185 by *Eco*RI digestion, yielding the construct pNM-H327A (*21*).

Preparation of Protein Samples. *Pa*-NiR was purified according to the method of Parr and co-workers (*22*). The preparation was judged pure when the oxidized enzyme had a 411 nm/280 nm ratio ≥1.1, and the protein concentration was determined using $\epsilon_{411\ nm} = 141\ mM^{-1}\ cm^{-1}$ for the oxidized protein (which refers to the concentration of active sites). The expression and purification of mutant *Pa*-NiR enzymes have been described previously (*21*). The recombinant protein is isolated as a "semi-apo" enzyme, in which the *c*-heme is incorporated but the d_1-heme is lacking. The "semi-apo" *Pa*-NiR H327A was judged pure when the reduced enzyme had a 417 nm/280 nm ratio of ≥1.3, and an $\epsilon_{417\ nm} = 139\ mM^{-1}\ cm^{-1}$ was used to determine the "semi-apo" protein concentration. *Pa*-NiR H327A was reconstituted with d_1-heme which had been extracted from the wild-type protein using the method of Walsh et al. (*23*). Concentrated samples of *Pa*-NiR H237A contained in 50 mM potassium phosphate buffer, pH 7.0, were incubated with a 1.5 stoichiometric excess of d_1-heme for 1 h at 16 °C. The samples were then eluted through small G25 columns equilibrated with the same buffer to remove the excess d_1-heme.

Stopped-Flow and Equilibrium Experiments. Both the stopped-flow and equilibrium CO binding experiments were carried out under anaerobic conditions in 100 mM potassium phosphate, pH 7.0, containing 1 mM EDTA at 20 °C. For stopped-flow experiments, protein samples were prepared by reducing the enzyme (5 μM) with sodium ascorbate (1 mM final concentration) in a tonometer. Following complete reduction, the protein sample was rapidly mixed with buffer containing various concentrations of CO (1−0.1 mM), ensuring that all reactions were carried out under pseudo-first-order conditions. The reaction was monitored using either a diode array detector (TN 6500 Tracor Northern, Madison, WI) or an Applied Photophysics stopped-flow apparatus; when single wavelength acquisition was used, the reaction was generally followed at 460 nm. Time courses were analyzed using the computer program MATLAB (The Math Works Inc., South Natick, MA). For the equilibrium CO binding experiments, *Pa*-NiR (7 μM) was placed in a capped cuvette, and the gas phase was excluded. Buffer containing 1 mM CO was introduced with a Hamilton syringe through the septum of the cuvette, and the absorbance spectrum of the sample after each addition was measured using a Jasco V-550 spectrophotometer.

Laser Photolysis Experiments. The laser experiments were carried out using two different laser apparatuses; however, both instruments used are very similar, and we describe one experimental setup. The light flash emitted by a pulsed Nd:YAG laser (200 mJ at 532 nm in 5 ns half-width duration Gaussian pulses) is focused onto a fluorescence cuvette sealed to a modified Thunberg tube containing 2.5 mL of a 8−10 μM solution of the enzyme equilibrated with 1 atm of pure CO. The transmittance of the sample is continuously monitored using the light beam of a 300 W lamp collimated onto the sample cuvette at 90° with respect to the laser light pulse. Opposite the lamp a Spex 1680 monochromator removes scattered laser light and transmits monochromatic light to a Hamamatsu R1398 fast response photomultiplier tube connected to a Hamamatsu C1053 current to voltage amplifier. The output of the amplifier is read by a Tektronix TDS360 digital oscilloscope, and the trigger for the oscilloscope is provided by a fast photodiode transiently illuminated by the laser light pulse transmitted through the sample cuvette. The crude voltage readings are converted into absorbance changes with respect to the pretrigger level (absorbance of *Pa*-NiR−CO) and further analyzed by a nonlinear least-squares minimization routine using either MATLAB (The Math Works Inc.) or Facsimile (AEA Techology, UK). The described experimental setup has a dead time of approximately 250 ns; therefore, no geminate ligand rebinding such as that seen with myoglobin (Mb) or hemoglobin (Hb) (*24*) can be observed. The recovery of photolyzed *Pa*-NiR can be calculated to be 30% of the total enzyme (see the results below).

RESULTS

Stopped-Flow and Static Titration Experiments. In the stopped-flow apparatus, *Pa*-NiR (2.5 μM after mixing) was rapidly mixed with various concentrations of CO under anaerobic conditions (50−500 μM after mixing). The time courses were monoexponential at all CO concentrations studied, and the rate was linearly dependent on the ligand concentration. At high CO concentrations, the full expected absorbance change was observed, and the data were fitted to a single-exponential function yielding a second-order rate constant $k_{on} = 2 \times 10^4\ M^{-1}\ s^{-1}$. At lower CO concentrations, the enzyme was not fully saturated, and therefore the data were fitted to Model 1.

Model 1

$$\text{reduced NiR} + \text{CO} \underset{k_{off}}{\overset{k_{on}}{\rightleftharpoons}} \text{reduced-NiR−CO}$$

This analysis yielded a $k_{off} = 0.12\ s^{-1}$ and a calculated equilibrium K_d of 6 μM. Equilibrium CO binding experiments revealed that the Hill coefficient is approximately 0.8 and the dissociation constant is 7 μM. The kinetic and equilibrium results agree well with each other, and the kinetic constants determined are in good agreement with those previously published (*25*, *26*). However, the observations that at all studied CO concentrations ligand binding is monoexponential and that the Hill coefficient is below unity are at variance with previously published results (*25*); the reasons for these discrepancies are unknown. CO binding experiments were also carried out on *Pa*-NiR H237A; at the studied

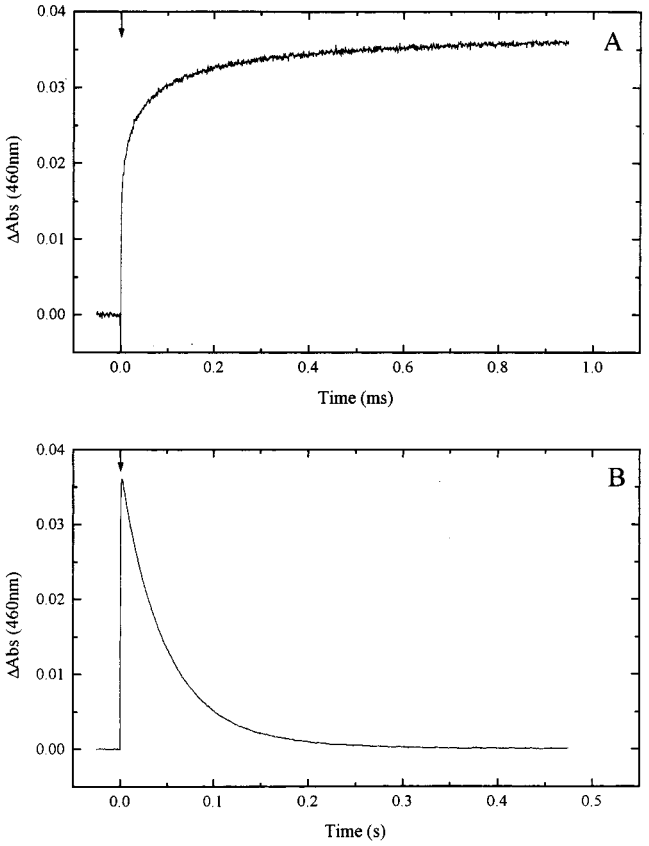

FIGURE 2: Transients seen in laser photolysis experiments of reduced CO-bound *Pa*-NiR. The reactions were carried out under anaerobic conditions in 50 mM potassium phosphate buffer, pH 7.0, containing 1 mM CO and at ambient temperature. Panel A: Microsecond relaxations monitored at 460 nm after photolysis of the fully reduced CO complex. The pre-trigger absorbance represents that of the fully reduced CO-bound *Pa*-NiR (8 μM), and this value has been set to zero. The reaction was initiated by photodissociation of CO with a laser pulse at 532 nm (denoted by the arrow). With the experimental design used, approximately the first 500 ns after the laser pulse is prone to artifacts and should not be considered part of the transient. Panel B: Time course of CO recombination to fully reduced *Pa*-NiR (8 μM). The reaction was initiated by photodissociation of CO (panel A); the laser flash is denoted by the arrow and recombination from the bulk was monitored at 460 nm.

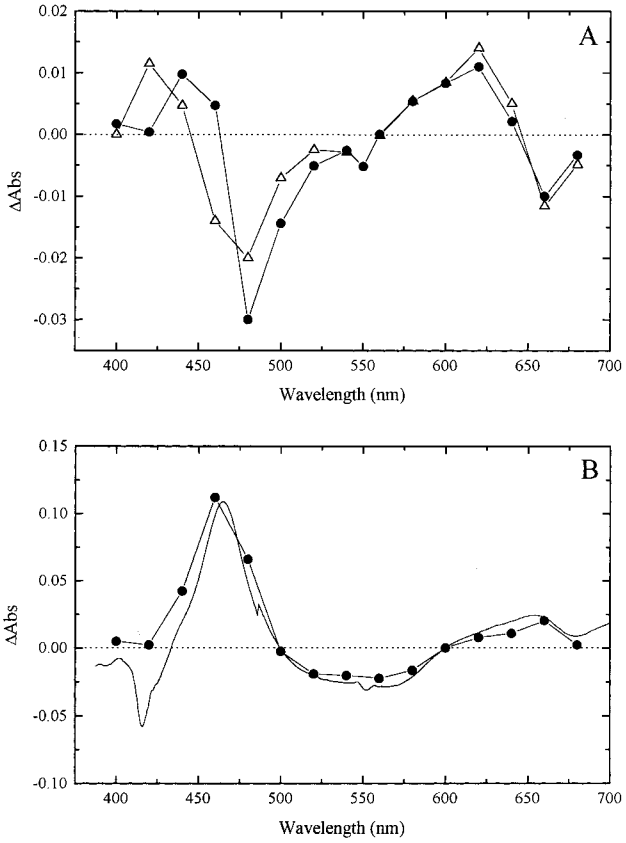

FIGURE 3: Optical difference spectra of the transients. Panel A: The combined amplitude of both microsecond phases seen after CO photodissociation from fully reduced wild-type *Pa*-NiR (△) and *Pa*-NiR H327A (●) is plotted as a function of wavelength. The concentration of *Pa*-NiR was 8 μM, that of *Pa*-NiR H327A was 10 μM, and the concentration of CO was 1 mM. Panel B: The static difference spectrum of reduced *Pa*-NiR *minus* reduced CO-bound *Pa*-NiR (solid line) is compared with the kinetic difference spectrum of the recombination reaction of CO with reduced wild-type *Pa*-NiR (see Figure 3, panel B) after normalization for protein concentration and for the extent of photolysis. We estimate that we have approximately 30% photolysis as determined from comparison between the static and kinetic difference spectra. Experimental conditions are reported in the legend of Figure 2.

wavelengths, the time courses were monoexponential, and the corresponding second-order rate constant (k_{on}) was 11 $\times$ 10^4 M^{-1} s^{-1}, which is significantly higher than that of the wild-type protein.

Laser Photolysis on Fully Reduced CO-Bound Pa-NiRs. Laser flash photolysis experiments conducted on the fully reduced CO-bound *Pa*-NiR revealed that upon CO dissociation the enzyme undergoes fast relaxations on a microsecond time scale. Since no absorption changes were observed on photoexcitation of the oxidized or unliganded reduced protein, these kinetic processes must be assigned to events occurring as a result of the photodissociation of CO. Figure 2 (panel A) shows the time evolution of absorbance at the d_1-heme Soret band after photolysis. At least two kinetic constants are needed to fit the time course, and their values, which are independent of ligand concentration, are reported in Table 1. The numerical analysis of these processes revealed that the rate constants are significantly correlated to each other; as a consequence, all fitted parameters are associated with significant errors (up to 30%; see Table 1) which are not independent of each other. Therefore, we did

Table 1: Rate Constants for Conformational Relaxations, CO Binding, and Internal eT for Wild-Type *Pa*-NiR and *Pa*-NiR H327A[a]

enzyme *Pa*-NiR	redox state	μs structural relaxation 1 ($\times 10^4$ s^{-1})	μs structural relaxation 2 ($\times 10^3$ s^{-1})	CO binding ($\times 10^4$ M^{-1} s^{-1})	μs eT ($d_1^{2+} \rightarrow c^{3+}$) ($\times 10^4$ s^{-1})
wild-type	fully reduced	3.0 $\pm$ 0.45	2.5 $\pm$ 0.75	2 (2)	
wild-type	mixed valence				2.5 $\pm$ 0.3
H327A	fully reduced	3.0 $\pm$ 0.45	2.5 $\pm$ 0.75	14 (11)	
H327A	mixed valence				3.5 $\pm$ 0.3

[a] The numbers in parentheses were determined by stopped-flow; all others were calculated from laser photolysis experiments. The reactions were carried out under anaerobic conditions in either 100 mM or 50 mM potassium phosphate buffer, pH 7.0.

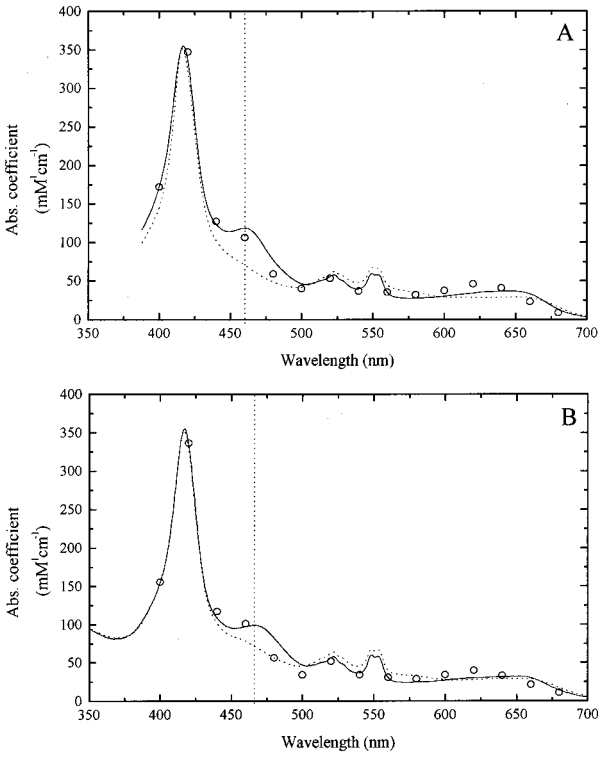

FIGURE 4: Static and kinetic absorption spectra of wild-type *Pa*-NiR (panel A) and *Pa*-NiR H327A (panel B). The solid line represents the spectrum of the fully reduced protein, the dotted line is the fully reduced CO-bound protein, and the open circles represent the spectrum of the intermediate populated immediately after the photodissociation of CO. In panel A, the vertical dotted line is at 460 nm while in panel B it is at 466 nm, indicating a red shift of the reduced d_1-heme γ band in *Pa*-NiR H327A. Experimental conditions are reported in the legend of Figure 2.

not attempt to assess the individual amplitude associated with each phase of the reaction, and only the total amplitude of the microsecond kinetic phases has been plotted as a function of wavelength (Figure 3, panel A). Clearly the kinetic difference spectrum shows that the microsecond kinetic processes do not represent CO recombination to the reduced d_1-heme (Figure 3). An alternative approach to the data analysis would be the use of a "stretched" exponential expression to describe the data. The rationale behind this assumption is that the photolyzed sample is made up of many nonequivalent *Pa*-NiR molecules each assuming a slightly different structural conformation (*27*, *28*). This hypothesis suggests that the observed kinetic phases cannot be correlated to a process where all the *Pa*-NiR molecules undergo two distinct conformational changes; rather, a large number of unrelaxed "substrates" converge, each with its own rate constant, to a smaller number of (or single) equilibrium unliganded states. Although we have not analyzed our data with a "stretched" exponential, we acknowledge that this approach may be of interest when more extensive data are available.

Following the microsecond phases, a much slower and second-order process is seen (Figure 2, panel B). Both the second-order rate constant (2×10^4 M^{-1} s^{-1}), which is identical to that measured for CO binding in the stopped-flow experiments, and the kinetic difference spectrum of this phase (Figure 3, panel B) indicate that it corresponds to rebinding of the unliganded reduced enzyme with CO diffusing from the bulk.

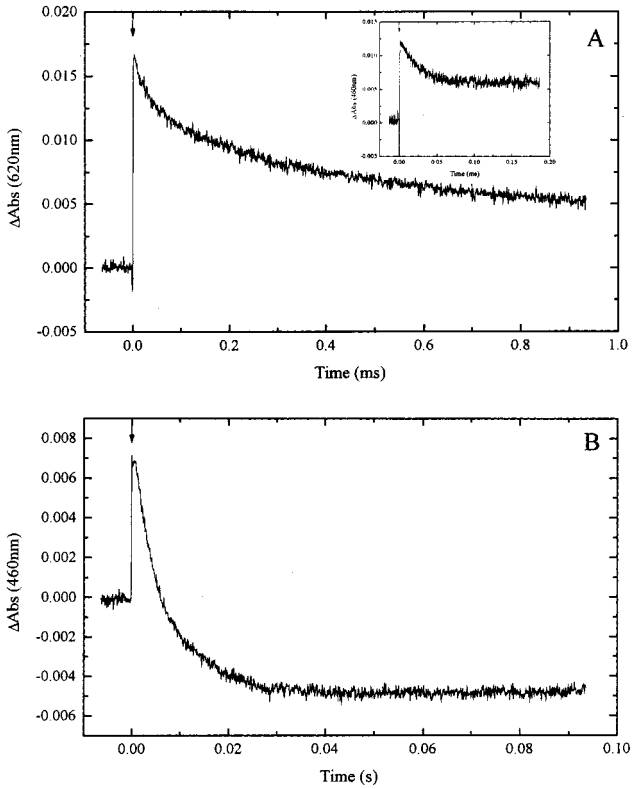

FIGURE 5: Transients seen in laser photolysis experiments of reduced CO-bound *Pa*-NiR H327A. The concentration of enzyme was 10 μM, and all other experimental conditions are reported in the legend of Figure 2. Panel A: Microsecond relaxations monitored at 620 nm after photolysis of the fully reduced CO complex of *Pa*-NiR H327A. The reaction was initiated by laser photodissociation of CO from the protein (laser flash is denoted by the arrow). The inset graph shows the same reaction monitored at 460 nm. Panel B: Time course of CO recombination to fully reduced *Pa*-NiR H327A. The reaction was initiated by the photodissociation of CO from the protein (panel A), the laser flash is denoted by the arrow, and the recombination from the bulk was monitored at 460 nm.

We have extended these experiments to the mutant *Pa*-NiR H327A. The static spectrum of fully reduced *Pa*-NiR H327A mutant (Figure 4) clearly shows that the γ band of the reduced d_1-heme, which in the wild-type protein is at 460 nm, is red-shifted by about 6 nm, to 466 nm, presumably a result of the mutation.

The time courses after CO dissociation from fully reduced *Pa*-NiR H327A were complex, and two phases were again observed in the microsecond time regime (Figure 5, panel A). A good description of the time course was obtained in a global fit of the microsecond relaxations for both the wild-type *Pa*-NiR and *Pa*-NiR H327A, using the same rate constants [$(3.0 \pm 0.45) \times 10^4$ s^{-1} and $(2.5 \pm 0.75) \times 10^3$ s^{-1}; see Table 1]. The kinetic difference spectra of the microsecond processes are shown in Figure 3, panel A; although the difference spectra of the wild-type and mutant *Pa*-H327A are rather similar in shape, there are some clear-cut differences, notably at 420 nm and more significantly at 460 nm. However, inspection of the absolute spectra of the unrelaxed species of both the wild-type and the mutant protein shows that they are very similar (Figure 4). Therefore, the differences observed in the difference spectra (Figure 3, panel A) are presumably a consequence of the reduced

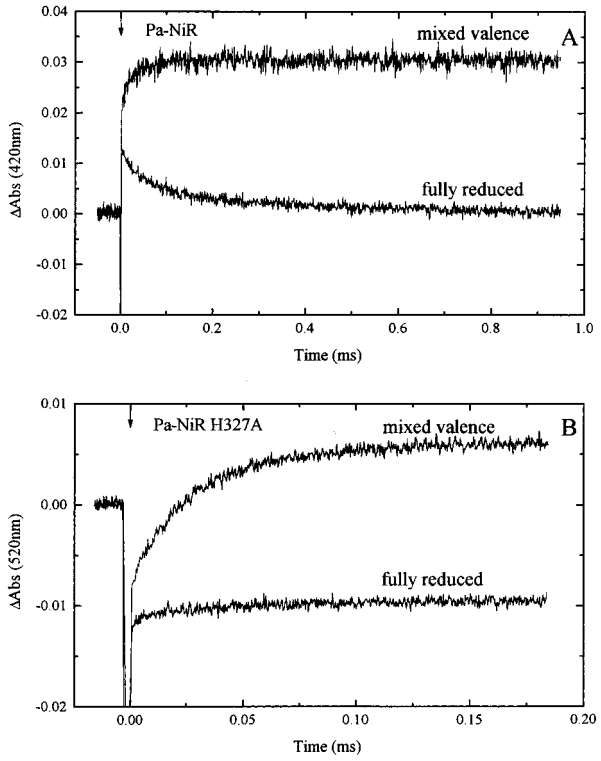

FIGURE 6: Kinetics of internal $d_1 \rightarrow c$ eT triggered by photolysis of CO (denoted by the arrow) from reduced d_1-heme. The concentration of enzyme was 10 μM, and all other experimental conditions are reported in the legend of Figure 2. Panel A: Microsecond absorbance changes monitored at 420 nm after laser photodissociation of CO, either from the mixed valence or from the fully reduced wild-type *Pa*-NiR. Panel B: Microsecond absorbance changes monitored at 520 nm after laser photodissociation of CO, either from the mixed valence or from the fully reduced *Pa*-NiR H327A.

spectra of the two proteins at equilibrium being different (as shown in Figure 4).

The CO rebinding to *Pa*-NiR H327A as observed in laser-flash experiments (Figure 5, panel B) was 7-fold faster than that observed in the wild-type protein. The agreement between the stopped-flow experiments and the photolysis experiments was fairly good; however, the rate of CO rebinding after photolysis was slightly faster than that observed in the stopped-flow (see Table 1). It was also noted that at a number of wavelengths the CO recombination transients were best fitted using a double exponential with rate constants of 190 and 50 s^{-1}; the reason for this biphasic behavior is not known and was not investigated further. Following CO rebinding to the mutant protein, an additional very slow phase was observed. At the wavelengths that the measurements were done, this phase represented approximately 10% of the total amplitude apart from at 420, 460, and 580 nm where the amplitude was more significant (approximately 35%). This reaction has not been assigned, but it could represent a number of processes, such as a slow structural alteration after CO rebinding, as previously observed in *Pa*-NiR (*21*). Other possibilities are that a small fraction of *c*-heme is able to bind CO and the slow phase is the recombination of CO to the *c*-heme after photolysis, or that we have a heterogeneous population of protein molecules due to the reconstitution of *Pa*-NiR H327A with d_1-heme.

Photolysis of the Mixed Valence Hybrids. The mixed valence hybrids of wild-type *Pa*-NiR and *Pa*-NiR H327A

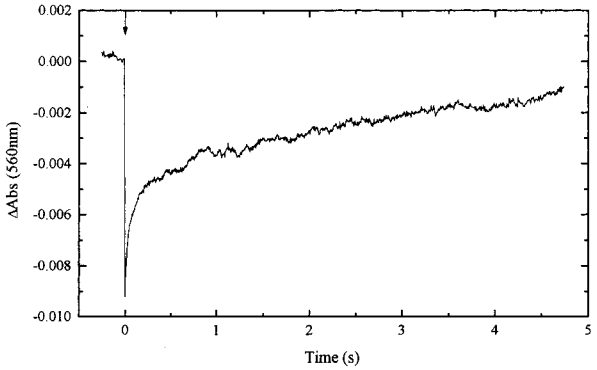

FIGURE 7: Time course of CO recombination to a mixed valence derivative of wild-type *Pa*-NiR, followed at 560 nm. The reaction was triggered by laser photodissociation (denoted by the arrow) of CO from the ferrous d_1-heme, the *c*-heme being ferric. The concentration of enzyme was 10 μM, and all other experimental conditions are reported in the legend of Figure 2.

were prepared by the addition of a 4-fold excess of potassium ferricyanide to the CO-bound fully reduced derivative. Due to the large redox potential difference between the CO-bound d_1-heme and the *c*-heme, only the *c*-heme was oxidized, which leads to population of the species c^{3+} d_1^{2+}−CO, as observed spectrophotometrically. Unfortunately, in the wild-type *Pa*-NiR this derivative is somewhat unstable (since CO is a reductant), and within some minutes it reverts back to the fully reduced CO-bound state. Therefore, the experiments must be carried out rapidly after addition of ferricyanide. The rate of eT from the unliganded ferrous d_1-heme to the ferric *c*-heme was followed by monitoring absorbance changes at 420 nm (a wavelength where the *c*-heme mainly contributes) on a microsecond time scale after CO photodissociation. Figure 6 (panel A) shows the time course of the absorbance changes observed after photolysis for the fully reduced and mixed valence hybrid; the latter displays an increase in absorbance at 420 nm indicative of *c*-heme reduction (rate constant = 2.5×10^4 s^{-1}), while the fully reduced protein exhibits the fast structural relaxations with an amplitude of opposite sign.

The mixed valence experiments were repeated on the *Pa*-NiR H327A mutant, which yielded a markedly more stable mixed valence state. The absorbance changes at 460, 520, and 550 nm followed on a microsecond time scale after CO photodissociation are consistent with synchronous d_1-heme oxidation and *c*-heme reduction (Figure 6, panel B), and can be fitted with a single exponential (at all three wavelengths) yielding a rate constant of 3.5×10^4 s^{-1}.

Laser photolysis experiments of mixed valence wild-type *Pa*-NiR showed that CO rebinding from the bulk was markedly biphasic, see Figure 7 (rate constants are 11 and 0.25 s^{-1}).

DISCUSSION

CO Binding to Fully Reduced Pa-NiRs. The CO recombination with the fully reduced *Pa*-NiR reported in this study is second order and slow, with $k = 2 \times 10^4$ M^{-1} s^{-1}, as obtained both by stopped-flow and by laser photolysis, and in good agreement with previously published results (*25*, *26*). Moreover, the kinetic difference spectrum is the same in the two experiments and compares well with the static spectrum. The fact that the rate constant for CO recombination is the

same regardless of the method used to initiate the reaction is important as it shows that the photoproduct of the laser photolysis has relaxed to a species indistinguishable from equilibrium reduced unliganded *Pa*-NiR prior to recombination with bulk CO. As discussed below, this is fully consistent with the microsecond conformational relaxations. The recombination of CO with the mutant *Pa*-NiR H327A is at least 5 times faster than with the wild-type protein. We correlate this increase with the removal of the bulky histidine residue sitting just above the d_1-heme (Figure 1). Site-directed mutagenesis of Mb has shown that the nature of the distal residues alters both the extent of geminate rebinding and the second-order rate constant for ligand recombination from the bulk (*29*). The almost invariant distal His (E7) gates access to the heme and is a major determinant of the second-order rate constant for recombination which increases 10-fold by substitution of His with Ala or Gly. Therefore, a decreased barrier to ligand diffusion in the *Pa*-NiR H327A mutant may well explain the 5-fold increased second-order rate constant for CO recombination. The crystallographic structure of reduced *Pa*-NiR (*12*) shows that His327 is 4 Å away from the iron atom of the d_1-heme and may be responsible for some hindrance to ligand diffusion to and from the heme, even though this residue is somewhat further away from the heme iron than His E7 is in Mb.

Fast Absorbance Changes after Photolysis of CO from Pa-NiRs. The microsecond relaxations observed after photolysis of the fully reduced CO complex do not have the kinetic difference spectrum characteristic of CO binding and are independent of CO concentration. Our interpretation is that the photoproduct is an unstable intermediate which decays to its equilibrium conformation with perturbations of the optical spectrum of the d_1-heme. It may be an oversimplification to assume that these structural changes can be assigned to motions of individual residues within the d_1-heme distal pocket. They may well reflect more global structural changes, for example, involving the *c*-domain loop which moves upon d_1-heme reduction and is coupled to a rotation of Tyr10 (*6*, *12*) (Figure 1). Our interpretation is that the microsecond transients observed with *Pa*-NiR are protein conformational relaxations similar to those proposed for the much better characterized structural relaxations observed in photolyzed Hb and Mb (*27*, *28*, *30*, *31*). As reported for these proteins, the structural relaxation of the photoproduct of *Pa*-NiR is complex as it cannot be described by a single-exponential process (Figure 2). We have refrained from analyzing the decay using a stretched exponential model (*27*, *28*), without necessarily implying that the two rate constants used to describe the time course reflect separate physical events.

The wild-type *Pa*-NiR and *Pa*-NiR H327A exhibit different optical spectra since the 460 nm band characteristic of the wild-type reduced protein is red-shifted by 6 nm in *Pa*-NiR H327A (Figure 4). Red shifts of the visible spectra of hemes have been explained in terms of a decrease in polarity of their binding pocket (*32*), which is consistent with the case of *Pa*-NiR H327A where the polar His327 has been replaced with a hydrophobic Ala side chain. More importantly, the spectrum of the transiently populated species recorded after photolysis is the same for the wild-type and mutant proteins (Figure 4). These results suggest that in CO-liganded *Pa*-NiR, His327 is somewhat displaced from the

Scheme 1

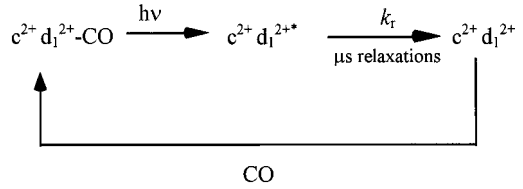

Scheme 2

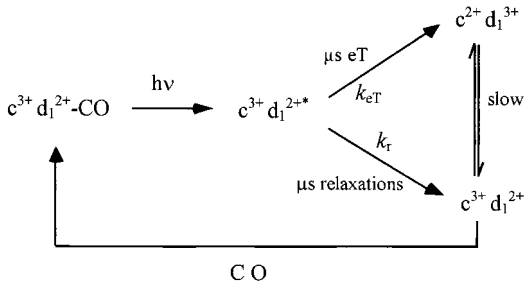

d_1-heme pocket, thereby diminishing its influence on the spectrum. The spectrum of the kinetic intermediate and its decay are very similar for both proteins, suggesting that the microsecond relaxations cannot be attributed solely to His327 relaxing back into position (see Figure 2, panel A).

Internal Electron Transfer. In the mixed valence derivative, the $d_1 \rightarrow c$ intramolecular eT is observed both in *Pa*-NiR H327A and in wild-type *Pa*-NiR (Figure 6). Since this reaction overlaps in time with the structural relaxations described above, it is likely to involve a partially or totally unrelaxed derivative, rather than the equilibrium state. Two experimental observations emerging from the interpretation of the time courses of the photolyzed mixed valence hybrids will be discussed: i.e., (i) the rate and absorbance changes associated with the fast eT; and (ii) the biphasic time course for CO rebinding from the bulk. Schemes 1 and 2 illustrate our proposed mechanism for the photochemically induced reactions in fully reduced and mixed valence *Pa*-NiR derivatives. For both the fully reduced and mixed valence *Pa*-NiR derivatives, photolysis yields an unliganded active site (denoted as $d_1{}^{2+}$*) which undergoes structural relaxations before CO rebinding from the bulk. We propose that in the mixed valence species (Scheme 2) only the transiently populated $d_1{}^{2+}$* form of the enzyme is able to rapidly reduce the ferric *c*-heme (microsecond eT, k_{eT}) and this reaction competes with the conformational relaxations occurring without changes in redox state distribution (k_r). The scheme assumes that the eT reaction is essentially irreversible, implying a large driving force between the species $c^{3+}d_1{}^{2+}$* and $c^{2+}d_1{}^{3+}$. Also for simplicity we have illustrated that $c^{3+}d_1{}^{2+}$* decays to $c^{2+}d_1{}^{3+}$ in a single process (k_{eT}) involving the eT event, although we may envisage two elementary processes (i.e., eT transfer and structural relaxations).

The rate constant of the microsecond processes ($d_1 \rightarrow c$) eT (Scheme 2) has been estimated as 2.5×10^4 s^{-1} and 3.5×10^4 s^{-1} in wild-type *Pa*-NiR and *Pa*-NiR H327A, respectively. This corresponds to the sum of the rate constants for eT and structural relaxations (Scheme 2). For both proteins, the direction of the absorbance change implies synchronous *c*-heme reduction and d_1-heme oxidation; however, it is difficult to assess whether the experimentally observed absorbance changes correlate well with the extent

of eT dictated by the difference in redox potentials and extinction coefficients between the two species. Apart from the complexity due to the unrelaxed d_1^{2+}* state (as shown in Scheme 2) being able to decay by two pathways, the driving force for the reaction is unknown, and only partial photolysis (≈30%) was obtained. Nevertheless, the data very clearly show that at key wavelengths, the mixed valence photolyzed species displays a kinetic behavior different from that of the fully reduced protein and consistent with eT from the reduced d_1-heme to the oxidized *c*-heme.

Following the microsecond eT and structural relaxations illustrated in Scheme 2, the resulting mixture of two slowly interconverting species ($c^{3+}d_1^{2+}$ and $c^{2+}d_1^{3+}$) would, in the absence of CO, equilibrate according to their redox potentials. However, in the presence of excess CO, which binds only to $c^{3+}d_1^{2+}$, biphasic recombination kinetics (Figure 7) are observed. The fast phase (11 s^{-1} at [CO] = 1 mM) is assigned to rebinding of bulk CO with the relaxed species $c^{3+}d_1^{2+}$ because this rate constant is similar to that expected for the fully reduced wild-type *Pa*-NiR. Since CO cannot rebind to the $c^{2+}d_1^{3+}$ species, reduction of the d_1-heme is mandatory, and thus CO combination is rate-limited by eT from the reduced *c*-heme, producing a rate constant = 0.25 s^{-1}. This hypothesis is consistent with previous stopped-flow experiments which, by following the kinetics of the reduction of *Pa*-NiR in the presence of excess reduced azurin, yielded an identical slow internal eT rate constant of 0.25 s^{-1} (*5*).

Structural Interpretation. It is now possible to speculate about the structural interpretation of some of the transient species, as the 3D structure of *Pa*-NiR has been solved for the oxidized, reduced, reduced-NO, and mixed valence $c^{2+}d_1^{3+}$ states (*6*, *12*, *14*). Reduction of *Pa*-NiR is associated to large structural changes, which are a concerted movement of a *c*-domain loop, a rotation of Tyr10 away from the active site, and the loss of the OH^- as the oxidized d_1-heme's sixth ligand (see Figure 1). However, the distance between the two hemes and their relative orientation do not change between the oxidized and reduced derivatives, and therefore changes in eT cannot be attributed to a change in the distance (*33*). The crystallographic data obtained on the $c^{2+}d_1^{3+}$ derivative are particularly interesting because they show that in this mixed valence state, the d_1-heme domain has a structure like the oxidized enzyme (*14*), suggesting that reduction of the d_1-heme is required for the structural changes to take place. With this in mind, it is reasonable to suggest that the equilibrium $c^{3+}d_1^{2+}$ species in Scheme 2 has a structure similar to that of the reduced protein. Therefore, the eT from $c^{2+}d_1^{3+}$ to $c^{3+}d_1^{2+}$ should involve a structural reorganization in which Tyr10 vacates the active site and OH^- dissociates from the Fe. The reverse eT step (i.e., $d_1 \rightarrow c$) is expected to be comparably slow, because the redox potentials of both hemes are very similar (*19*, *20*), resulting in an equilibrium constant close to unity. Moreover, stopped-flow experiments which monitored the oxidation of d_1-heme determined this internal eT rate constant as 0.35 s^{-1} (*5*). Therefore, the $d_1 \rightarrow c$ eT rate is very different when the electron donor is either the equilibrium structure of *Pa*-NiR or the unrelaxed transient state ($c^{3+}d_1^{2+}$*). It is tempting to suggest that this difference in rate is due to the structural difference between the two species. The structure of $c^{3+}d_1^{2+}$* is, of course, unknown, but given the microsecond spectral perturbations illustrated above, it cannot be identical to the equilibrium conformation (*6*, *12*). Therefore, we postulate that the transient species is able to transfer an electron very rapidly, while the equilibrium form, due to a lower driving force and/or to an increase in the reorganizational energy term linked to structural changes, transfers an electron slowly. The data reported above suggest that photodissociation experiments in single crystals of CO-bound *Pa*-NiR, if possible, may provide direct evidence for the dynamics of the ligand-linked structural changes by time-resolved X-ray diffraction (*34*).

ACKNOWLEDGMENT

We express our thanks to C. Cambillau and M. Tegoni (Marseille, France) for their suggestions about the structural dynamics of *Pa*-NiR and also to L. Federici and A. Miele (University of Rome, Italy) for their assistance with the preparation of Figure 1.

REFERENCES

1. Silvestrini, M. C., Falcinelli, S., Ciabatti, I., Cutruzzolà, F., and Brunori, M. (1994) *Biochimie 76*, 641−654.
2. Cutruzzolà, F. (1999) *Biochim. Biophys. Acta* (in press).
3. Averill, B. A. (1996) *Chem. Rev. 96*, 2951−2964.
4. Zumft, W. G. (1997) *Microbiol. Mol. Biol. Rev. 61*, 533−616.
5. Parr, S. R., Barber, D., Greenwood, C., and Brunori, M. (1977) *Biochem. J. 167*, 447−455.
6. Nurizzo, D., Silvestrini, M. C., Mathieu, M., Cutruzzolà, F., Bourgeois, D., Fülöp, V., Hajdu, J., Brunori, M., Tegoni, M., and Cambillau, C. (1997) *Structure 5*, 1157−1171.
7. Fülöp, V., Moir, J. W. B., Ferguson, S. J., and Hajdu, J. (1995) *Cell 81*, 369−377.
8. Silvestrini, M. C., Colosimo, A., Brunori, M., Walsh, T. A., Barber, D., and Greenwood, C. (1979) *Biochem. J. 183*, 701−709.
9. Silvestrini, M. C., Tordi, M. G., Musci, G., and Brunori, M. (1990) *J. Biol. Chem. 265*, 11783−11787.
10. Horio, T., Higashi, T., Sasagawa, M., Kusai, K., Nakai, M., and Okunuki, K. (1960) *Biochem. J. 77*, 194−201.
11. Yamanaka, T., Ota, A., and Okunuki, K. (1961) *Biochim. Biophys. Acta 53*, 294−308.
12. Nurizzo, D., Cutruzzolà, F., Arese, M., Bourgeois, D., Brunori, M., Cambillau, C., and Tegoni, M. (1998) *Biochemistry 37*, 13987−13996.
13. Williams, P. A., Fülöp, V., Garman, E. F., Saunders, N. F. W., Ferguson, S. J., and Hajdu, J. (1997) *Nature 389*, 406−412.
14. Nurizzo, D., Cutruzzolà, F., Arese, M., Bourgeois, D., Brunori, M., Cambillau, C., and Tegoni, M. (1999) *J. Biol. Chem. 274*, 14997−15002.
15. Brzezinski, P., and Wilson, M. T. (1997) *Proc. Natl. Acad. Sci. U.S.A. 94*, 6176−6179.
16. Greenwood, C., Barber, D., Parr, S. R., Antonini, E., Brunori, M., and Colosimo, A. (1978) *Biochem. J. 173*, 11−17.
17. Bellelli, A., Brzezinski, P., Arese, M., Cutruzzolà, F., Silvestrini, M. C., and Brunori, M. (1996) *Biochem. J. 319*, 407−410.
18. Kobayashi, K., Koppenhofer, A., Ferguson, S. J., and Tagawa, S. (1997) *Biochemistry 36*, 13611−13616.
19. Schichman, S. A., and Gray, H. B. (1981) *J. Am. Chem. Soc. 103*, 7794−7795.
20. Silvestrini, M. C., Tordi, M. G., Colosimo, A., Antonini, E., and Brunori, M. (1982) *Biochem. J. 203*, 445−451.
21. Cutruzzolà, F., Arese, M., Grasso, S., Bellelli, A., and Brunori M. (1997) *FEBS Lett. 412*, 365−369.
22. Parr, S. R., Barber, D., Greenwood, C., Phillips, B. W., and Melling J. (1976) *Biochem. J. 157*, 423−430.
23. Walsh, T. A., Johnson, M. K., Barber, D., Thomson, J., and Greenwood, C. (1980) *J. Inorg. Biochem. 14*, 15−31.

24. Gibson, Q. H. (1989) *J. Biol. Chem. 264*, 20155−20158.
25. Parr, S. R., Wilson, M. T., and Greenwood, C. (1975) *Biochem. J. 151*, 51−59.
26. Wharton, D. C., and Gibson, Q. H. (1976) *Biochim. Biophys. Acta 430*, 445−453.
27. Ansari, A., Berendzen, J., Bowne, S. F., Frauenfelder, H., Iben, I. E. T., Sauke, T. B., Shyamsunder, E., and Young, R. D. (1985) *Proc. Natl. Acad. Sci. U.S.A. 82*, 5000−5004.
28. Hagen, S. J., Hofrichter, J., and Eaton, W. A. (1995) *Science 269*, 959−962.
29. Springer, B. A., Silgar, S. G., Oslon, J. S., and Phillips, J. N. (1994) *Chem. Rev. 94*, 699−714.
30. Sawicki, C. A., and Gibson, Q. H. (1976) *J. Biol. Chem. 251*, 1533−1542.
31. Henry, E. R., Jones, C. M., Hofrichter, J., and Eaton, W. A. (1997) *Biochemistry 36*, 6511−6528.
32. Platt, J. R. (1956) in *Radiative Biology* (Hollaender, A., Ed.) McGraw-Hill, New York.
33. Marcus, R. A., and Sutin, N. (1985) *Biochim. Biophys. Acta 811*, 265−322.
34. Srajer, V., Teng, T., Ursby, T., Pradervand, C., Ren, Z., Adachi, S., Schildkamp, W., Bourgeois, D., Wulff, M., and Moffat, K. (1996) *Science 274*, 1726−1729.

BI990179U